Available online at www.sciencedirect.com

ScienceDirect

Procedia Manufacturing 53 (2021) 500–506

Procedia MANUFACTURING

www.elsevier.com/locate/procedia

49th SME North American Manufacturing Research Conference, NAMRC 49, Ohio, USA

Novel riser designs via 3D sand printing to improve casting performance

Md Moinuddin Shuvo[a] and Guha Manogharan[a,*]

[a]*Department of Mechanical Engineering, The Pennsylvania State University, State College, PA, 16802, United States*

* Corresponding author. Tel.: 814-863-7273; *E-mail address:* gum53@psu.edu

Abstract

3D sand printing (3DSP) has created a new era for sand casting applications by introducing additively manufactured complex 3D sand molds and cores. It has also enabled the design and manufacturing of complex rigging (gating and feeding) systems using non-conventional design rules which were not previously feasible. In this research, two novel riser designs, ellipsoid and spherical risers, along with traditional cylindrical risers are investigated to understand their effects on the solidification time and entrained air volume fraction in Aluminum alloy (A319) castings. Computational simulations are presented to understand the viability of complex riser shapes by comparing critical parameters such as fluid temperature during filling, solidification, and cooling. In addition, solid fraction (SF) and entrained air volume fraction are also studied during filling and solidification. The results for spherical riser performance showed a 7% increase in feeding time during solidification along with a 47.27% reduction in entrained air volume fraction. The ellipsoid riser studied in this research also showed identical solidification time at half the volume of the conventional cylindrical riser. This indicated a 26.5% increase in casting yield. These riser designs will not only facilitate the design optimization of the casting but also improve the casting performance (feeding, solidification) for difficult to cast materials and geometries.

Keywords: 3D sand-printing; Sand casting; Additive manufacturing; Metal casting; Feeding system; Risers

1. Introduction

Metal casting is one of the oldest manufacturing techniques with significant advantages over other manufacturing processes due to its ability to rapidly produce parts with complex geometries out of any alloy. The most common casting process is sand casting, which has over 60% of the metal casting market share [1]. Although sand casting has been around for thousands of years, the underlying physics of 3D sand casting has largely remained unchanged until recently. Researchers have recently established guidelines for 3D rigging design and successfully cast metal parts with significantly lower defects and improved mechanical properties [2–5]. While sand casting is a well-established technique, it has been revolutionized by new developments, most notably 3D Sand Printing (3DSP) [6]. 3DSP is a binder jetting additive manufacturing process that involves printing sand molds and cores layer by layer (e.g. furan binder to process foundry silica sand). 3DSP offers new opportunities to enable highly complex, low-volume mold production with intricate shapes, sizes, and features [7,8].

Sama et al. presented a comparative study between 3DSP and traditional sand-casting technology [2,3]. While traditional sand casting requires permanent tooling for fabrications, 3DSP eliminates these requirements and can rapidly produce molds and cores using “virtual” pattern [9]. This reduces the number of steps required in the casting process which reduces the lead time for small batches of molds. In addition, commercially available foundry consumables can be integrated into the 3D Sand Printers [10,11]. 3DSP not only reduces the lead time during casting but also reduces the CO_2 emissions and can incorporate design optimizations in both molds and cores [12].

The sand casting process is mainly divided into two systems, the gating system, and the feeding system. While the gating system incorporates the components and passageways that enable the molten metal to enter the mold cavity, the feeding system supplies metal after the filling of the casting during solidification [13,14]. A schematic

10.1016/j.promfg.2021.06.052

representation of the conventional 2D gating and feeding system is represented in Figure 1. One of the essential aspects of the feeding system is the riser. Risers are primarily integrated into metal casting operations to counteract the shrinkage during solidification. They act as molten metal reservoirs by supplying metal to eliminate porosity and defects due to shrinkage. While risers are well accepted as an integral element of the feeding system, there is a fundamental knowledge gap in the design methodologies for complex 3D risers for different metals and alloys, placement of the risers, and sleeves. In addition, risers also act as a passageway for entrained air to leave the casting if they are open to the atmosphere. The crucial design parameters that govern the effectiveness of a riser are riser geometry, placement, number of risers, feeding distance, riser neck shape, and size, and filling patterns of the cast [13,15].

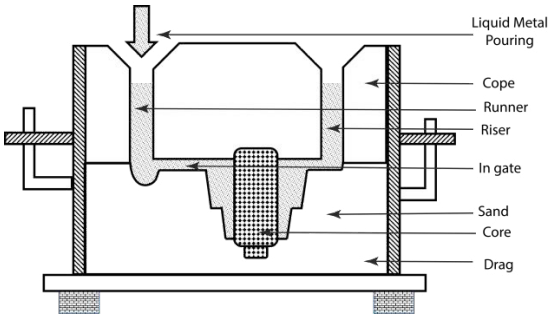

Figure 1: Schematic of the conventional gating and feeding system components in sand casting process

According to Chorinov's rule for riser design, the riser must have a higher volume to area ratio (also known as thermal modulus) than the casting it is feeding in order to have a higher solidification time [16]. From the geometric analysis, it is already known that spheres have the highest volume to area ratio compared to any other shapes with similar volume [17]. As such, spherical risers are the most efficient and optimal riser shape for any casting. However, spherical risers could not be incorporated into conventional molds previously because of their complex shape. Since 3DSP can produce complex sand molds, it is now possible to create spherical as well as other complex riser shapes. In addition, prior studies on risers focused exclusively on the steel industry [15]. As new materials are being introduced with different mechanical properties, it is important to establish the design framework for optimum gating and feeding system design across alloys.

In this research, two novel risers were analyzed, ellipsoid and spherical risers, and benchmarked against traditional cylindrical risers. A quantitative analysis has been presented for these risers at two important locations of interest in the casting on melt temperature during filling, solidification, and cooling. In addition, solid fraction, entrained air volume fraction during solidification and filling were also studied based on results from simulations. The material used in this study was Aluminum alloy A319. The results from this research indicated that the spherical riser was superior with longer feeding time (7% increase), lower entrained air volume fraction (~48% decrease), and lower solid fraction (4% decrease) when compared against the traditional cylindrical riser. In addition, a 26.5% increase in casting yield was found in the case of the ellipsoid riser. The spherical riser also achieved lesser turbulence at the probe locations when the melt fills the riser. This research also draws attention to further investigation of the instantaneous change in effective riser geometry due to solidification shrinkage and how it affects the thermal modulus of the riser.

2. Materials and Methods

2.1 Materials

The material used in this study is Aluminum alloy A319 with a pouring temperature of 737°C. The composition of the material is listed in Table 1 [18]. The sand mold used for the simulation was furan bonded silica sand.

Table 1. Chemical composition (%wt) of Aluminum alloy A319 used in this study [18]

Si	Fe	Mn	Cu	Mg	Ti	Zn	V
5.78	0.43	0.29	3.75	0.05	0.03	0.06	0.011

During solidification simulations, the default parameters for the material properties were used for A319 and are listed in Table 2.

Table 2. Metal pouring and mold properties

Parameter	Value
Pouring Temperature	737°C
Surface tension coefficient	0.914 kg/s2
Solidus temperature	504°C
Liquidus temperature	610°C
Latent heat of fusion	4e+05 J/kg
Furan Sand Specific heat	1.763e+06 Kg/m/s^2/° C
Furan Sand Thermal conductivity	0.511 W/m/°C
Metal flow velocity at in-gate	0.5 m/s

2.2 CAD Designs

Figure 2 represents the CAD designs of the cast part. The dimension of the part was benchmarked from a well-established study on risers by Nandi et al. [19]. The volume across all the designs was kept constant with changes only to the surface area between the riser designs. The volume of the

risers for all the designs was 67347.89 mm^3, while the surface area for the risers were different for all three risers. The surface area and volume of the three different shapes are listed in Table 3.

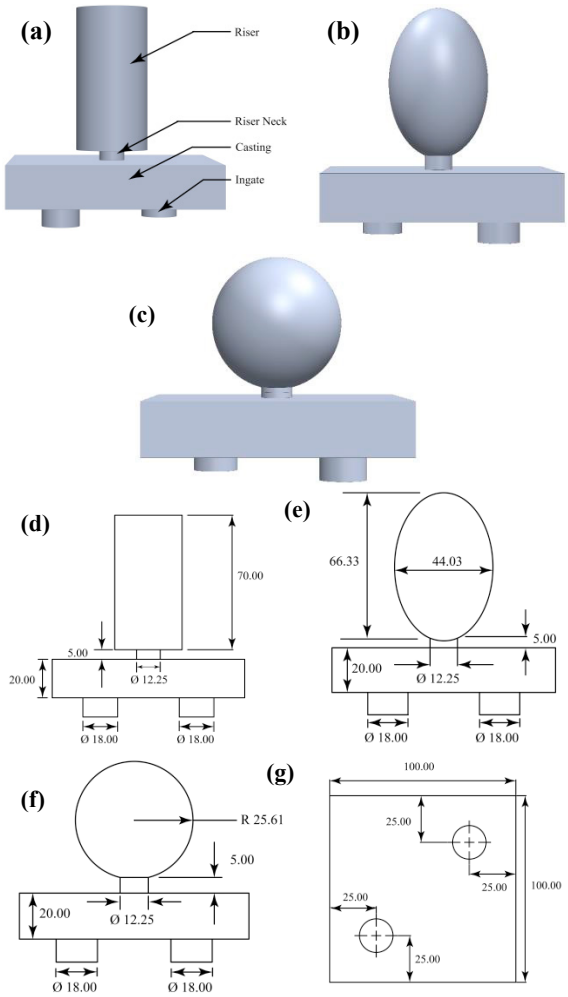

Figure 2: CAD drawings and dimensions (mm) of traditional cylindrical (a, d), ellipsoid (b, e) and spherical risers (c, f), and benchmark castings (g)

Table 3. Table 3: Surface area and riser volumes

Shape of the riser	Area (mm^2)	% Area Reduction	Volume (mm^3)
Cylindrical	9621.13	-	67347.89
Ellipsoid	8231.71	14.44	
Spherical	8005.10	16.80	

2.3 Simulation Setup

The simulation software used in this study was FLOW-3D Cast v5.0 (Santa Fe, NM) with a cell mesh size of 1 mm. Three simulations per riser design were conducted. The governing equations used by the solver are mass continuity equation, momentum equation, and energy equation. A general scalar transport model has been used which includes particle tracing, air entrainment, and fluid residence time. Flow-3D uses the "Fractional Area/Volume Obstacle Representation (FAVOR)" method that offers computationally more efficient mesh generation and numerical algorithms [20]. Convective and radiative heat transfer from the fluid to the void regions has been incorporated into the simulations by Newton's law of cooling and Stefan-Boltzmann's law. The latent heat of the fluid is considered by specifying the solidus and liquidus temperature. The latent heat is removed linearly with a change in solidification temperature [21]. The density of the material was set as a function of temperature with the adiabatic gas region for the gas mode. The boundary conditions were set up as constant temperature of 25°C and the *y*-max (open to atmosphere) boundary was atmospheric gas pressure of 101325 Pa. The time step in the simulation was automatically set by the solver and it ranged from .001s at the beginning of filling to 0.149s towards the end of solidification. As shown in Figure 2(a), two ingates were positioned at the bottom of the cast with a constant inlet velocity of 0.5m/s for the metal to flow inside the cavity which is the criteria for succinctly filling the metal through 3D rigging that can be achieved via 3D sand-printing [14,22]. Two probes were set at two different locations of the riser to record process conditions (temperature, entrained air volume, solid fraction, etc.) during the entire simulation run as shown in Figure 3. Since the riser neck has a lower cross-sectional area than the riser, in most cases it solidifies earlier in the process. Hence, probe 1 was located in the riser neck. Probe 2 was located at 20 mm above probe 1 where the molten metal is expected after solidification shrinkage has occurred inside the riser.

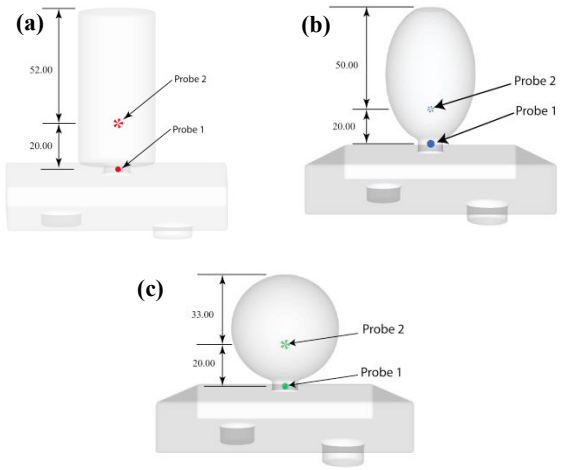

Figure 3: Probe locations in: (a) cylindrical, (b) ellipsoid and (c) spherical risers

3. Results and Discussion

3.1 Melt Filling

Figure 4 shows the temperature profile at probe 1 (neck of the riser). The molten metal reaches the spherical riser faster when compared to the other two riser cases. The probe reads a temperature of 610°C as soon as the molten metal reaches the neck region. The time of entrance of molten metal at probe location 1 are 2.29s, 2.36s, and 2.55s for the spherical, ellipsoid, and cylindrical riser, respectively. The sudden drop of temperature at 3.14s for the ellipsoid riser is due to the flow separation created in the neck region at that time instance due to turbulence which was observed in all three runs. Figure 5 shows the temperature distribution from the flow simulation with the neck region highlighted where the separation occurred.

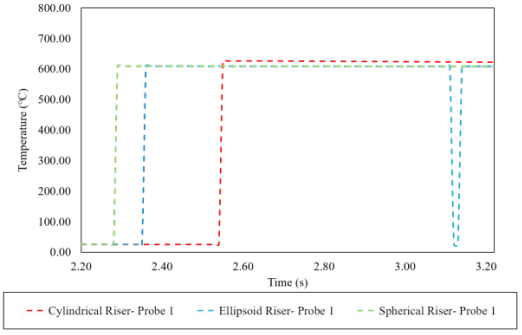

Figure 4: Temperature at probe 1 during filling

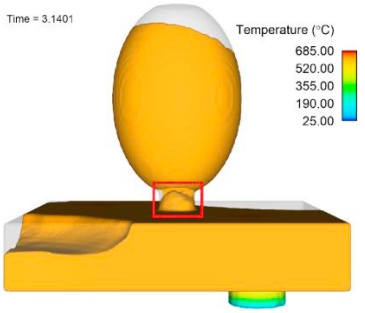

Figure 5: Temperature distribution of casting at time 3.14s during filling in ellipsoid riser

The velocity profile at the two probe locations during filling is presented in Figure 6. At probe 1, which is in the neck region, maximum velocity is recorded for the ellipsoid riser and minimum velocity is observed in the spherical riser. From the literature review, it was found that an in-gate velocity higher than 0.5 m/s suffers from turbulence and the creation of bi-film in the liquid metal [23]. However, since risers are not part of the final casting, this criterion should be evaluated for risers. But, it is evident that lower turbulence and melt velocity during filling of risers is desired to improve feeding of metals back into the casting. In the case of the spherical riser at 2.75s, both of the probes read the same velocity of 0.65 m/s and remain unchanged till 3.22s when the riser is completely filled. At 2.93s for the cylindrical riser, probe 1 reports a velocity of 0.67 m/s, whereas probe 2 reports a velocity of 0.77 m/s. The ellipsoid riser experiences similar velocities at both the probes with a magnitude of 0.74 m/s. The spherical riser experiences the least amount of turbulence resulting in the lowest overall velocity at the probes. Figure 7 represents the highlighted velocity distribution of the melt at time 3.14s during filling in the ellipsoid risers.

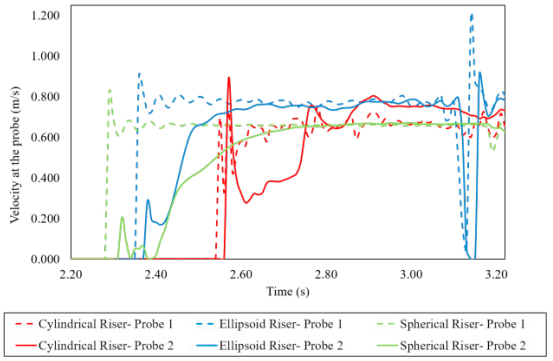

Figure 6: Velocity measurement at probes 1 and 2 during filling

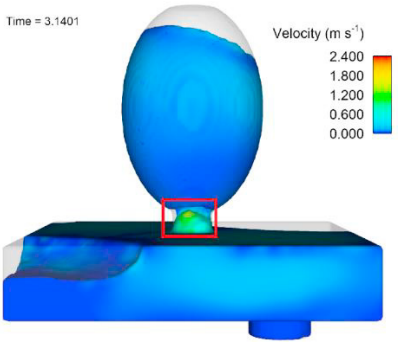

Figure 7: Velocity distribution of melt at time 3.14s during filling in ellipsoid riser

Figure 8 represents the entrained air volume fraction during filling. The spherical riser in this case experiences the lowest entrained air volume fraction (0.4%). At 3s, the entrained air volume fraction for cylindrical riser is 0.95% and for spherical riser 0.50%. This indicates a 47.26% reduction in the entrained air volume fraction for the spherical riser. Figure 9 shows the turbulence in ellipsoid riser experiences the largest air volume fraction at 3.14s. The

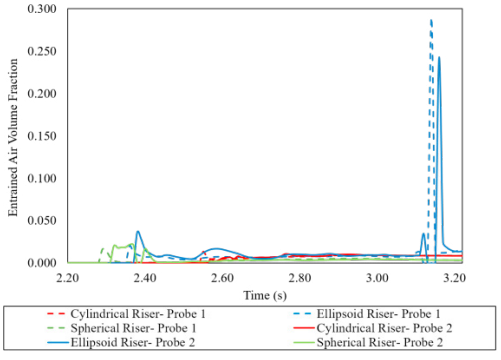

Figure 8: Entrained air fraction in the castings during filling

initial turbulence occurs when the molten metal enters the riser through the riser neck which increased entrained air volume fraction in between 2.3s to 2.4s across all the risers.

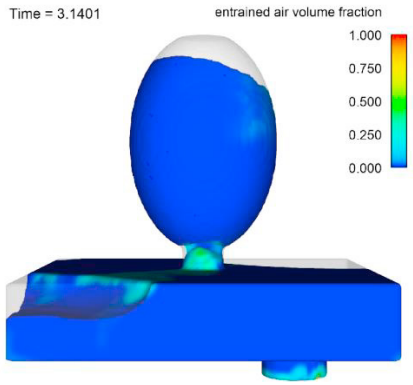

Figure 9: Entrained air volume in ellipsoid riser

3.2 Solidification

Figure 10 represents the solidification profile in the risers. The solidification starts right after the filling of the casting is completed and due to differences in filling velocity, starts at different timestamps (on an average difference of 3.5 seconds) between the different risers investigated in this study. The solidus temperature (the highest temperature at which an alloy is completely solid) for Aluminum A319 is 504°C and the liquidus temperature (the temperature at which an alloy is completely melted) is 610°C. The solidification starts with probes 1 and 2 both reporting a temperature of 610°C, which indicates that is filled with molten metal. Temperature values from probe 1 indicate that the neck region of the cylindrical riser solidifies faster when compared with the ellipsoid and spherical risers. At probe 1, it takes 62.97s, 65.12s, and 74.23s to reach solidus temperature in cylindrical, ellipsoid, and spherical risers, respectively. This is an improvement of 3.41% and 17.88% in ellipsoid and spherical risers, respectively when compared with cylindrical risers. At probe 2, the durations for reaching the solidus temperature are 122.87s, 112.47s, and 145.61s for the cylindrical, ellipsoid, and spherical risers, respectively.

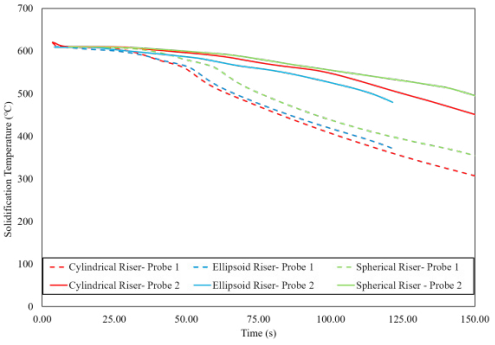

Figure 10: Solidification profile of the castings at probes 1 and 2 after filling

Although the ellipsoid riser should take more time than the cylindrical riser, the deviation from this happens due to a significant reduction in molten metal in the riser itself at the start of solidification as represented in Figure 11 (a) and (b). Almost half of the molten metal flows back to the cast from the ellipsoid and spherical riser to fill up the void space created during filling in the cast. This results in a shape that has a comparatively lower volume to area ratio than the cylindrical riser, which in turn results in a reduction of solidification time by 8.5%. In addition, a reduction of 0.0499kg of molten metal in the ellipsoid riser takes place during this process which results in a 26.5% increase in casting yield as less material is required during the initial filling stage.

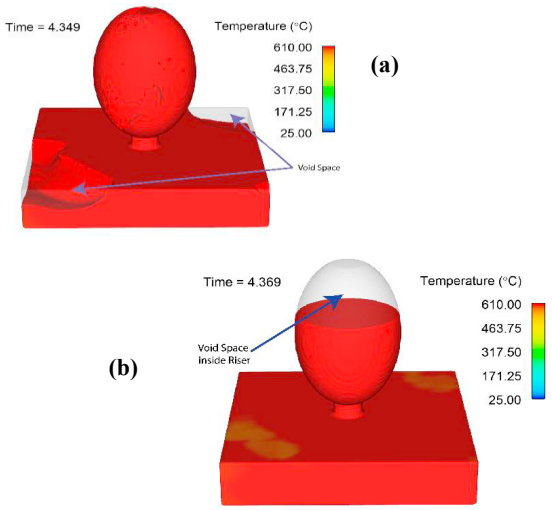

Figure 11: Temperature profile of ellipsoid risers during solidification (a) end of filling (b) start of solidification

Figure 12 illustrates the modified shape of the riser with the actual shape in shaded contrast for the three different types of the riser with the probe 2 temperature at 504°C.

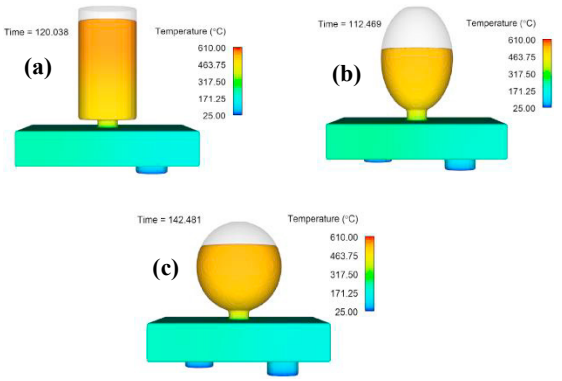

Figure 12: Successful filling of casting at liquidus temperature of 504°C (a) Cylindrical (b) Ellipsoid (c) Spherical

Figure 13 represents the solid fraction (SF) profile for all three risers. A solid fraction value of 1 represents all the molten metal in the probe region has reached the solidus state

from its initial liquidus state. The spherical riser requires the highest amount of time to reach the SF value of 1 for both probes. Figure 14 shows the SF contours for the different risers. Although the probe 2 reported SF values reach 1 for all the risers, there still exists molten metal on the top section of the risers with the SF value ranging from 0.75 to 0.9 in the cylindrical riser.

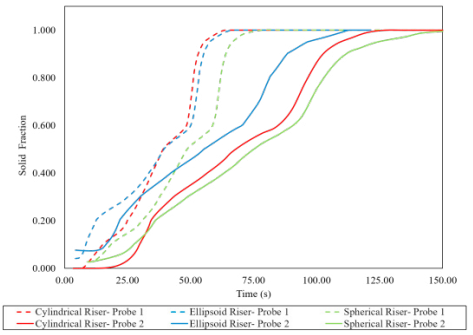

Figure 13: Solid fraction (SF) in the castings at probes 1 and 2 during solidification

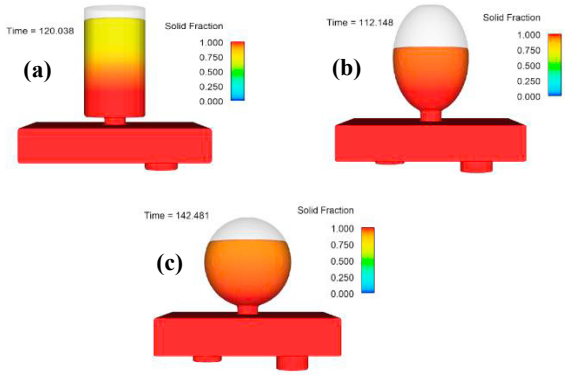

Figure 14: Solid fraction (SF) = 1 at probe 2 in castings with (a) Cylindrical (b) Ellipsoid (c) Spherical risers

3.3 Cooling

The cooling period starts after the solidification has been completed and the molten metal has reached the solidus temperature. The cooling phenomenon continues till the whole casting and the riser reach the room temperature of 25°C. All the cast sections along with the risers reach the room temperature within 1 hour after the filling, however, the initial cooling down temperature up to 100°C follows a different temperature profile as shown in Figure 15. It takes 429s, 375s, and 459s for cylindrical, ellipsoid, and spherical risers respectively to cool down to 100°C at probe position 2. Similar to solidification, the cooling time for the ellipsoid riser is also lower than the cylindrical riser due to its modified instantaneous shape right after the filling of void space.

Figure 16 represents the temperature profile at 100°C for probe location 2 for all the three risers. It is evident from these results that even with a reduced amount of molten metal in the risers, both ellipsoid and spherical risers are able to successfully feed cast metal during the solidification and cooling period. In addition, the spherical riser is able to provide 22.7s extra cooling time and a 7% improvement in feeding time during solidification when compared with traditional cylindrical risers.

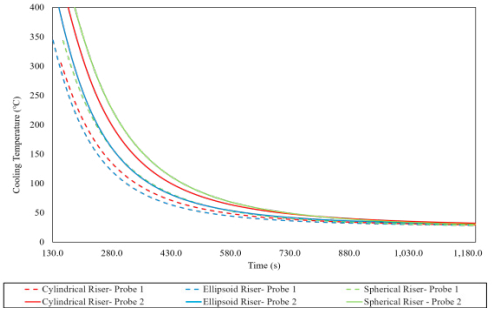

Figure 15: Temperature profile at probes 1 and 2 during cooling period

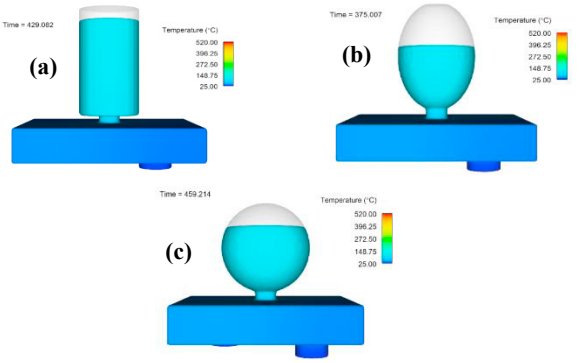

Figure 16: At 100°C, simulation shows successful cool down in (a) Cylindrical (b) Ellipsoid (c) Spherical risers

4. Conclusions

In this original research, two novel riser designs that are feasible only via 3D Sand-Printing were investigated and benchmarked against traditional cylindrical riser that is commonly used in conventional casting. Results from the simulations were analyzed to identify the impact of riser designs on filling, solidification, and cooling for Aluminum alloy A319 casting. Major conclusions from this study are:

- Both spherical and ellipsoid risers were successful in feeding the casting throughout solidification.
- A 7% improvement in feeding time during solidification can be achieved via the spherical riser.
- Spherical risers result in a 47.26% reduction in entrained air volume fraction in comparison to the cylindrical riser.
- Ellipsoid riser results in a 26.5% increase in casting yield.
- The ellipsoid riser was able to feed liquid metal to the cast effectively with a solidification time comparable to the cylindrical riser even after its thermal modulus

reduced significantly due to entrained filling in the initial stage.

- The spherical riser provided superior results in terms of velocity at the probes and entrained air volume fraction.

This research also draws attention to further investigation for the instantaneous shape change of the riser due to solidification shrinkage and how it affects the thermal modulus of the riser. While this study is limited to computational analysis, ongoing efforts of the authors include experimental validation including; embedded sensors to measure melt filling and solidification profile. Additional characterization via micro CT will also be conducted.

Acknowledgments

This research work was funded by NSF CMMI Award 1944120. The authors also thank Philip King and Ryan Stebbins for their help throughout the project.

References

[1] Rao, T. V. R., 2007, Metal Casting: Principles and Practice, New Age International.

[2] Sama, S. R., Wang, J., and Manogharan, G., 2018, "Non-Conventional Mold Design for Metal Casting Using 3D Sand-Printing," J. Manuf. Process., **34**, pp. 765–775.

[3] Sama, S. R., Badamo, T., Lynch, P., and Manogharan, G., 2019, "Novel Sprue Designs in Metal Casting via 3D Sand-Printing," Addit. Manuf., **25**, pp. 563–578.

[4] Dispinar, D., and Campbell, J., 2007, "Effect of Casting Conditions on Aluminium Metal Quality," J. Mater. Process. Technol., **182**(1–3), pp. 405–410.

[5] Campbell, J., 2015, Complete Casting Handbook: Metal Casting Processes*, Metallurgy, Techniques and Design*, Butterworth-Heinemann.

[6] Schwab, K., 2017, The Fourth Industrial Revolution, Currency.

[7] Wang, J., Sama, S. R., and Manogharan, G., 2019, "Re-Thinking Design Methodology for Castings: 3D Sand-Printing and Topology Optimization," Int. J. Met., **13**(1), pp. 2–17.

[8] Hackney, P. M., and Wooldridge, R., 2017, "Characterisation of Direct 3D Sand Printing Process for the Production of Sand Cast Mould Tools," Rapid Prototyp. J., **23**(1), pp. 7–15.

[9] Sama, S. R., Badamo, T., and Manogharan, G., 2020, "Case Studies on Integrating 3D Sand-Printing Technology into the Production Portfolio of a Sand-Casting Foundry," Int. J. Met., **14**(1), pp. 12–24.

[10] Woods, K., Giese, S., and Trikha, S., 2019, "Feasibility of US Foundry Supply Chain Consumables for Three-Dimensional Sand Printing," Int. J. Met., **13**(3), pp. 500–503.

[11] Lynch, P., Hasbrouck, C., Wilck, J., Kay, M., and Manogharan, G., 2020, "Challenges and Opportunities to Integrate the Oldest and Newest Manufacturing Processes: Metal Casting and Additive Manufacturing," Rapid Prototyp. J., **26**(6), pp. 1145–1154.

[12] Sivarupan, T., Upadhyay, M., Ali, Y., El Mansori, M., and Dargusch, M. S., 2019, "Reduced Consumption of Materials and Hazardous Chemicals for Energy Efficient Production of Metal Parts through 3D Printing of Sand Molds," J. Clean. Prod., **224**, pp. 411–420.

[13] Sutaria, M., Joshi, D., Jagdishwar, M., and Ravi, B., 2011, "Feeding System Design and Evaluation Using Temperature Gradient (Feed Path) Maps," Am. Foundry Soc., **9**.

[14] King, P., Martinez, D., and Manogharan, G. P., 2020, "Novel Sprue Designs to Reduce Casting Defects in Nickel-Aluminum Bronze: A Computational Study," ASME International.

[15] Carlson, K. D., Hardin, R. A., Ou, S., and Beckermann, C., 2002, "Development of New Feeding-Distance Rules Using Casting Simulation: Part I. Methodology," Metall. Mater. Trans. B, **33**(5), pp. 731–740.

[16] Ravi, B., 2005, Metal Casting: Computer-Aided Design and Analysis, PHI Learning Pvt. Ltd.

[17] Shouzhu, O. U., Carlson, K. D., and Beckermann, C., 2005, "Feeding and Risering of High-Alloy Steel Castings," Metall. Mater. Trans. B Process Metall. Mater. Process. Sci., **36**(1), pp. 97–116.

[18] Kumar, S., and Tewari, S. P., 2018, "Metallurgical and Mechanical Characterization of A319 Aluminum Alloy Casting Solidified Under Mold Oscillation," Int. J. Met., **12**(1), pp. 28–35.

[19] Nandi, T., Behera, R., Kayal, S., Chanda, A., and Sutradhar, G., 2011, "Optimization of Riser Size of Aluminium Alloy (LM6) Castings by Using Conventional Method and Computer Simulation Technique," Int. J. Sci. Eng. Res., **2**(11).

[20] Barkhudarov, M., "Advanced Simulation of the Flow and Heat Transfer Processes in Simultaneous Engineering," Citeseer, (Fig 1), pp. 1–15.

[21] *Flow Science, Inc., Santa Fe, NM, USA. FLOW-3D® Version 12.0 Users Manual (2018) [Online]*.

[22] Sama, MacDonald, Voigt, and Manogharan, 2019, "Measurement of Metal Velocity in Sand Casting during Mold Filling," Metals (Basel)., **9**(10), p. 1079.

[23] Runyoro, J., Boutorabi, S. M. A., and Campbell, J., 1992, "Critical Gate Velocities for Film-Forming Casting Alloys: A Basis for Process Specification," AFS Trans, **100**, pp. 225–234.